

UNCLASSIFIED

AD 268 786

*Reproduced
by the*

ARMED SERVICES TECHNICAL INFORMATION AGENCY
ARLINGTON HALL STATION
ARLINGTON 12, VIRGINIA



UNCLASSIFIED

NOTICE: When government or other drawings, specifications or other data are used for any purpose other than in connection with a definitely related government procurement operation, the U. S. Government thereby incurs no responsibility, nor any obligation whatsoever; and the fact that the Government may have formulated, furnished, or in any way supplied the said drawings, specifications, or other data is not to be regarded by implication or otherwise as in any manner licensing the holder or any other person or corporation, or conveying any rights or permission to manufacture, use or sell any patented invention that may in any way be related thereto.

CATALOGED BY ASTIA
AS AD No.

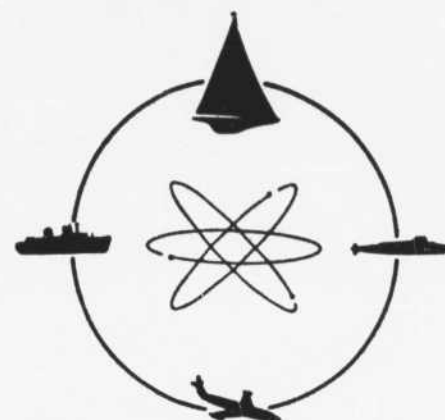
268786

268 786



STEVENS INSTITUTE
OF TECHNOLOGY

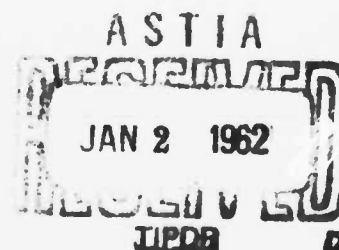
CASTLE POINT STATION
HOBOKEN, NEW JERSEY



DAVIDSON
LABORATORY

QUARTERLY PROGRESS REPORT APRIL - JUNE 1961
RESEARCH PROGRAM ON CONVERSION OF EXPLOSIVE ENERGY

Contract DA-28-017-501-ORD-3450
DL Project LB-2221



STEVENS INSTITUTE OF TECHNOLOGY

DAVIDSON LABORATORY
CASTLE POINT STATION
HOBOKEN, NEW JERSEY

QUARTERLY PROGRESS REPORT APRIL - JUNE 1961

RESEARCH PROGRAM ON CONVERSION OF EXPLOSIVE ENERGY

Contract DA 28-017-501-ORD-3450

DL Project LB-2221

Prepared by: S. J. Lukasik
S.J. Lukasik, Head
Fluid Physics Division

TABLE OF CONTENTS

| | Page |
|------------------------------------|------|
| SCOPE OF WORK..... | 1 |
| RESULTS OF WORK..... | 2 |
| A. Firings Conducted..... | 2 |
| B. Magnetic Field Work..... | 2 |
| C. Conductivity Measurement..... | 2 |
| D. Shaped Charges..... | 9 |
| WORK PLANNED FOR NEXT QUARTER..... | 14 |
| PERSONNEL..... | 15 |
| DISTRIBUTION LIST..... | 16 |

Quarterly Progress Report April - June 1961
Research Program on Conversion of Explosive Energy

Contract DA-28-017-501-ORD-3450
DL Project LB-2221

SCOPE OF WORK

During the past quarter the analysis of existing conductivity data has been completed and work on existing experimental programs has continued. The mechanical construction of the capacitor bank was completed and the checkout of its electrical performance began. Overall ringing measurements and inductance measurements on the various components are underway. Definitive results will be reported at a later time when the work is completed.

The conductivity measurements in unseeded charges are brought to a conclusion with a final tabulation of selected experimental results. These are based on the calibrated double-probe technique as well as the T-probe technique. Both techniques give results in Comp. B and pentolite that agree with each other and with the results of other investigators to within a factor of two. This is believed to be a measure of the absolute accuracy of this type of measurement at the present time. Measurements on Comp. B seeded with one percent concentrations of cesium and potassium compounds have shown no increase in the electrical conductivity of the detonating explosive.

The shaped charge collision work has continued. Jet collisions at a pressure of 0.1 mm Hg in a propane-flushed system have been observed with streak and framing cameras and by means of a prism spectrograph. The same brilliant luminosity that was observed in the jet collisions in air was again observed in a vacuum. Spectrographs of the air collision show a blackbody spectrum corresponding to a temperature of 6850°K on which is superposed a weak absorption spectrum. The same observations were made for a jet collision at low pressure. A considerably stronger and richer absorption spectrum was observed. Analysis of the spectrum has revealed the presence of many neutral and some ionized copper lines. Further analysis of the line shapes of the ionized copper lines is underway at the present time in an effort to infer the degree of ionization of the copper.

RESULTS OF WORK

A. Firings Conducted

During the past quarter five firings have been conducted. These are listed and briefly described in Table I.

B. Magnetic Field Work

During this quarter construction of the new capacitor bank was completed. A photograph of the assembled bank, together with the collector plate and transmission line to the spark gap switch is shown in Fig. 1. Protective armour plates which will insulate the capacitor bank from explosive forces and fragments are not shown. A trigger circuit to effect bank switching has been built and operated. This trigger circuit is designed for use in conjunction with the master control panel and electronic timing equipment existing at the Arsenal firing site. A checkout of the performance of the bank is now in progress; the results will be reported in a later report.

C. Conductivity Measurement

During this past quarter the work was directed toward a final reduction of existing conductivity firing data. The method of calculating load resistance during detonation from the first observed signal pulse, as described previously⁽¹⁾, was applied to all conductivity firings to date. Values of detonation zone resistivity were then obtained from the calculated resistance. For firings employing a double probe the resistivity, ρ_e , is calculated from

$$\rho_e = R_e / \left(\frac{R}{\rho} \right)_{cal}$$

where R_e is the measured load resistance during detonation and $(R/\rho)_{cal}$ is the probe calibration constant obtained from a separate calibration experiment⁽¹⁾. In most cases the double probe calibration constant $(R/\rho)_{cal}$ is obtained by averaging the three zero pulse length values for three different salt calibration solution depths. For situations where some of the calibration data were erratic, the irregular results were not used in calculating the calibration constant.

(1) Quarterly Progress Report, January - March 1961

Table I

| Firing No. | P.A. No. | Date | Type Charge | Optical Coverage | Purpose |
|------------|----------|--------|---|---|--|
| 97 | 1-1154 | 29 Mar | Opposed shaped charges | Framing camera | Observe jet collision in propane-flushed vacuum system; one detonation failed |
| 98 | 1-1155 | " | " | " | Repeat of 97 |
| 99 | 1-1173 | 15 Apr | " | Framing camera Streak camera Spectrograph | Observe jet collision in air. Observe spectrum of collision |
| 100 | 1-1183 | 27 Apr | " | " | Repeat of 97 with spectrum observation |
| 101 | 1-1192 | 9 May | Single shaped charge on a copper target | " | Observe jet-target collision in propane-flushed vacuum system. Observe spectrum of collision |

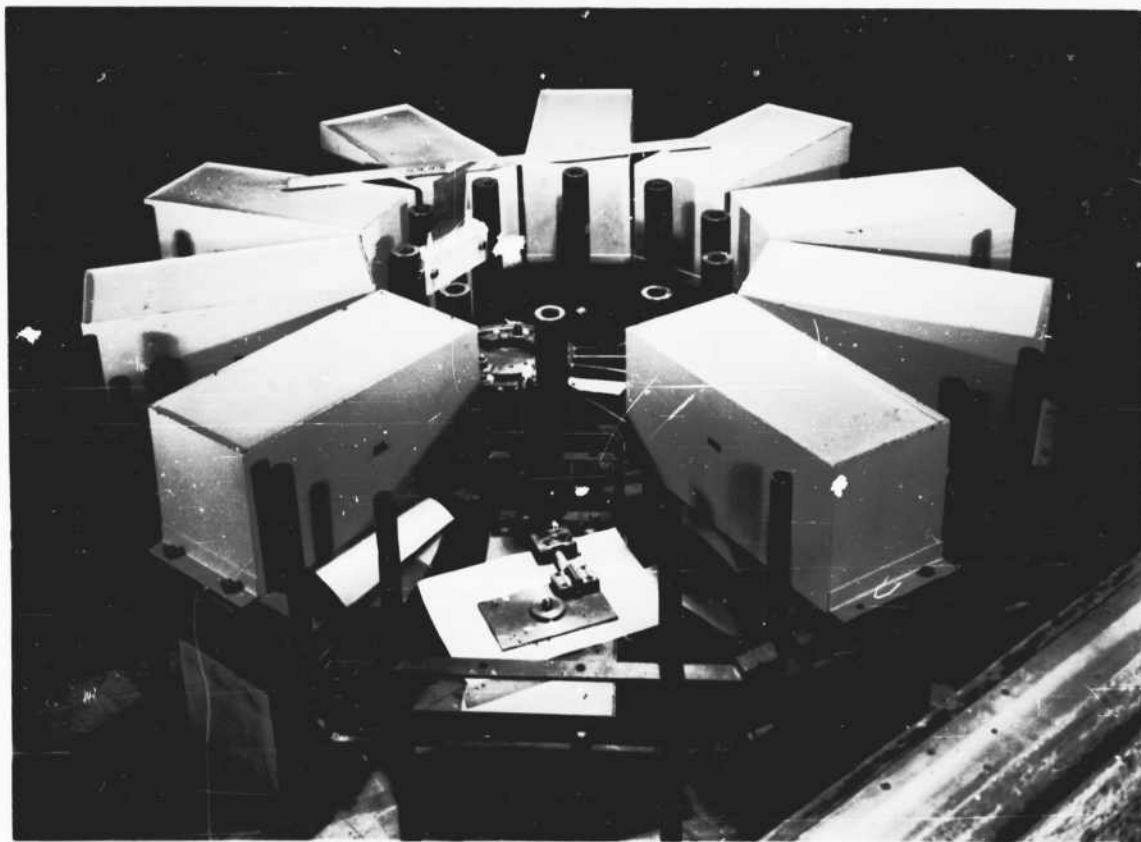


Figure 1

Assembled capacitor bank, including collector plate
and transmission line (spark gap switch and load
coil not shown)

For a T-probe the resistivity is calculated from

$$\rho_e = R_e \frac{h\ell}{d}$$

where d is the separation between T-probe electrodes, h the length of the electrode in contact with the explosive, and ℓ a length corresponding to either the probe thickness or an assumed reaction zone thickness. The detailed procedure for calculating resistivity from T-probe data is as follows. The electrical current distribution in the detonation zone and hence the measured probe resistance is influenced by both probe size and detonation zone geometry. Lacking detailed information on the geometry of the detonation zone, it is assumed to have the shape of a rectangular slab of constant resistivity; the dimensions of the slab are determined by the cross-sectional area of the explosive charge (h, d), and the unknown surface reaction zone length ℓ .

For a small T-probe thickness the measured resistance is assumed to be determined by the probe thickness rather than the reaction zone length. The consistency of measured resistance and calculated resistivity values of firings 42-c, 43-c, and 44-c, where the probe thickness is varied, are indicative of this dependence. An average value of explosive resistivity obtained from these three firings for Comp B is 0.33 ± 0.10 ohm cm. In situations where the T probe thickness is large, however, as in firing 37-c, the measured probe resistance depends upon the reaction zone length. Using the above average resistivity value, and the measured probe resistance of firing 37-c, a surface reaction zone length is computed, 0.18 ± 0.07 mm. This zone length is then used to calculate the explosive resistivity in the remaining firings where T probes were employed and Comp B was the explosive material. For Pentolite a reaction zone thickness of 0.25 mm is used in calculating the resistivity.

Table II is a summary of the results for all firings to date, indicating probe geometry and location, experimental operating conditions, measured resistance R_e , probe calibration $(R/\rho)_{cal}$ where applicable, calculated resistivity ρ_e , and estimates of the error in resistivity $\Delta\rho_e$ due to calibration variability and/or uncertainties in the data. A number of firings yielded either no results due to experimental difficulties or oscilloscope traces that were not readily interpretable.

Table 11
Final Summary of All Conductivity Firings and Results

| Firing No. | Date | Probe No. | Probe location | Atmos. | Confine. | Probe thickness (in.) | Explosive | Resistance R_e (ohm) | Error ΔR_e (ohm) | Comment | Calib. Const. $(R/\rho)_{cal}$ (cm^{-1}) | Comment | Resistivity ρ_e (ohm cm) | Error $\Delta \rho_e$ (ohm cm) |
|------------|------------|-----------|----------------|---------|----------|-----------------------|----------------------|------------------------|--------------------------|-------------------------|--|---------------------|-------------------------------|--------------------------------|
| 1 | 16 Dec '59 | (double) | surface | air | none | NA | Comp B | -- | -- | poor record | -- | no calibration | -- | -- |
| 2 | 9 Mar '60 | (T) | surface | air | yes | 0.019 | Comp B | -- | -- | poor record | NA | -- | -- | -- |
| 3 | 9 Mar | (T) | surface | air | yes | 0.019 | Comp B | -- | -- | poor record | NA | -- | -- | -- |
| 4 | 9 May | T | surface | air | yes | 0.019 | Comp B | -- | -- | no record | NA | -- | -- | -- |
| 5 | 9 May | T | surface | air | yes | 0.019 | Comp B | -- | -- | poor record | NA | -- | -- | -- |
| 6 | 17 June | T | surface | air | yes | 0.019 | Pent. | -- | -- | no record | NA | -- | -- | -- |
| 7 | 17 June | T | surface | air | yes | 0.019 | Pent. | -- | -- | no record | NA | -- | -- | -- |
| 8 | 19 July | T | surface | air | yes | 0.019 | Comp B | 10.4 | 3.4 | slow osc. sweep | NA | -- | 0.37 | 0.19 |
| 9 | 19 July | T | surface | air | yes | 0.019 | Comp B | 10.4 | 3.4 | slow osc. sweep | NA | -- | 0.37 | 0.19 |
| 10 | 19 July | T | surface | air | yes | 0.019 | Pent. | 10.4 | 3.4 | slow osc. sweep | NA | -- | 1.04 | 0.34 |
| 11 | 19 July | T | surface | air | yes | 0.019 | Pent. | 10.4 | 3.4 | slow osc. sweep | NA | -- | 1.04 | 0.34 |
| 12 | 20 July | T | surface | air | yes | 0.019 | Pent. | 11.3 | 5.0 | slow osc. sweep | NA | -- | 1.13 | 0.50 |
| 13 | 20 July | T | surface | air | yes | 0.019 | Pent. | 11.3 | 5.0 | slow osc. sweep | NA | -- | 1.13 | 0.50 |
| 14 | 20 July | 42 | surface | air | yes | NA | Pent. | -- | -- | no record | 3.72 | cal. questionable | -- | -- |
| 15 | 20 July | 43 | surface | air | yes | NA | Pent. | 12.8 | 7.5 | slow osc. sweep | 3.41 | cal. questionable | 3.76 | 2.20 |
| 16 | 20 July | 44 | surface | air | yes | NA | Pent. | 12.8 | 8.0 | slow osc. sweep | 41.8 | cal. questionable | 0.31 | 0.19 |
| 17 | 5 Aug | 45 | surface | air | yes | NA | Pent. | -- | -- | poor record | 80.4 | cal. questionable | -- | -- |
| 18 | 5 Aug | 46 | surface | air | yes | NA | Pent. | 114.0 | 17.0 | slow osc. sweep | 52.7 | cal. questionable | 2.16 | 0.32 |
| 19 | 5 Aug | 41 | surface | air | yes | NA | Pent. | 3.2 | 0.7 | slow osc. sweep | 3.84 | extensive cal. data | 0.83 | 0.26 |
| 20 | 5 Aug | T | surface | air | yes | 0.019 | Pent. | -- | -- | no record | NA | -- | -- | -- |
| 21 | 5 Aug | T | surface | air | yes | 0.019 | Pent. | 39.4 | 17.0 | slow osc. sweep | NA | -- | 0.98 | 0.43 |
| 22 | 2 Dec '60 | T | surface | propane | yes | 0.013 | Pent. | -- | -- | poor record | NA | -- | -- | -- |
| 23 | 6 Dec | 20 | surface | air | yes | NA | Comp B | 13.1 | 3.6 | -- | 9.28 | -- | 1.41 | 0.39 |
| 24 | 6 Dec | T | surface | propane | yes | 0.019 | Comp B | -- | -- | poor record | NA | -- | -- | -- |
| 25 | 6 Dec | T | surface | propane | yes | 0.019 | Comp B | 10.3 | 3.4 | -- | NA | -- | 0.37 | 0.19 |
| 26 | 9 Dec | T | surface | propane | none | NA | Comp B | -- | -- | no record | 8.61 | -- | -- | -- |
| 27 | 27 Dec | 4 | surface | propane | none | NA | Comp B | 20.3 | 2.8 | -- | 9.22 | cracked probe | 2.20 | 0.30 |
| 28 | 28 Dec | 12 | surface | propane | yes | NA | Comp B | 10.3 | 2.5 | -- | 10.79 | -- | 0.95 | 0.24 |
| 29 | 28 Dec | 13 | surface | propane | yes | NA | Comp B | -- | -- | poor record | 13.36 | -- | -- | -- |
| 30 | 3 Jan '61 | 17 | surface | propane | none | NA | Comp B | 13.8 | 2.2 | -- | 3.42 | poor cal. results | 4.04 | 0.65 |
| 31 | 3 Jan | 15 | surface | propane | none | NA | 1%CsClO ₄ | 16.1 | 4.8 | slow osc. sweep | 15.43 | poor cal. results | 1.04 | 0.31 |
| 32 | 4 Jan | 14 | surface | propane | none | NA | Pent. | 22.0 | 3.2 | -- | 12.33 | -- | 1.78 | 0.27 |
| 33 | 4 Jan | 16 | surface | propane | none | NA | Pent. | 14.3 | 2.2 | -- | 4.52 | poor cal. results | 3.16 | 0.50 |
| 34 | 9 Jan | 18 | surface | propane | none | NA | Comp B | -- | -- | zero volt. control exp. | -- | cracked probe | -- | -- |
| 35 | 9 Jan | 22 | surface | propane | none | NA | 1%CsClO ₄ | 21.8 | 4.3 | -- | 25.36 | -- | 0.86 | 0.17 |
| 36 | 10 Jan | 23 | surface | propane | none | NA | 1%KNO ₃ | 17.4 | 3.4 | -- | 10.99 | -- | 1.59 | 0.32 |
| 37 | 10 Jan | T | surface | propane | none | 0.065 | Comp B | 9.4 | 2.0 | -- | NA | -- | 0.33 | 0.10 |
| 38 | 11 Jan | 5 | internal | NA | NA | NA | Comp B | 8.0 | 1.9 | -- | 8.58 | -- | 0.93 | 0.23 |
| 39 | 11 Jan | 7 | internal | NA | NA | NA | Comp B | 6.7 | 1.9 | -- | 8.39 | -- | 0.80 | 0.23 |
| 40 | 11 Jan | 6 | internal | NA | NA | NA | Comp B | 10.3 | 1.9 | -- | 9.34 | -- | 1.10 | 0.21 |
| 41 | 12 Jan | T | surface | propane | none | 0.019 | Comp B | 7.4 | 1.0 | -- | NA | -- | 0.27 | 0.14 |
| 42 | 12 Jan | T | surface | propane | none | 0.015 | Comp B | 3.9 | 1.7 | -- | NA | -- | 0.30 | 0.13 |
| 43 | 12 Jan | T | surface | propane | none | 0.008 | Comp B | 8.8 | 2.0 | -- | NA | -- | 0.36 | 0.08 |
| 44 | 13 Jan | T | surface | propane | none | 0.005 | Comp B | 13.5 | 2.9 | -- | NA | -- | 0.34 | 0.08 |
| 45 | 13 Jan | T | surface | propane | none | 0.001 | Comp B | 8.0 | 2.5 | poor probe alignment | NA | -- | 0.04 | 0.01 |

The list of firings can be divided into two categories. Firing 1-c through 21-c were of an exploratory nature but they do yield some results. The remaining firings, 22-c through 45-c, incorporated a number of modifications intended to illustrate the dependence of detonation zone resistivity upon various parameters and to improve experimental technique. These modifications are:

1. change in probe mounting to minimize reaction zone confinement
2. use of propane to inhibit air-shock contamination
3. use of fast oscilloscope sweep to examine the leading edge of the signal pulse
4. use of double probes systematically calibrated
5. use of internal double probes to investigate the effect of probe location
6. variation of the T probe thickness as a means of measuring reaction zone thickness
7. use of seeded charges in an attempt to directly influence explosive resistivity

Table III is a grouping of double probe values given in Table II to illustrate and compare the effects of confinement, atmosphere, probe location, and seeding for Comp B, and to compare resistivity values for Comp B and Pentolite. The results for a number of firings are eliminated for reasons indicated in Table II.

Table III
Double Probe Resistivity Summary
(resistivity in ohm cm)

| | confined | | unconfined |
|--------------------------|--|------------|---|
| | Air | Propane | Propane |
| Comp B surface | 1.41(23-c)* | 0.95(28-c) | -- |
| Comp B internal | 0.93(38-c) 0.80(39-c) 1.10(40-c) | | |
| Comp B 1% seeded surface | | | Cs: 1.04(31-c) 0.86(35-c) K: 1.59(30-c) |
| Pentolite surface | 1.86** | | 1.78(32-c) |

* Number in brackets indicates firing from which data is obtained

** Weighted average of firings 15-c, 16-c, 18-c, 19-c

The above presentation indicates the following:

- (a) Internal and surface explosive resistivities are of the order of magnitude of one ohm cm.
- (b) There is good repeatability in resistivity values for Internal Comp B measurements.
- (c) The effect of air-shock induced conductivity as compared to propane atmosphere results in contrary to expectations; however any small difference that may exist is masked by the estimated error in resistivity.
- (d) 1% Cesium and 1% Potassium additives appear to have no effect upon explosive resistivity.
- (e) Resistivity values for Pentolite are about twice as large as that for Comp B.
- (f) The effects of confinement and atmosphere for Pentolite are not apparent, if present at all.

Table IV is a similar grouping of T probe values given in Table II again to illustrate and compare the effects of confinement and atmosphere for Comp B, and to obtain comparative resistivity values for Comp B and Pentolite.

Table IV

T Probe Resistivity Summary
(resistivity in ohm cm)

| | confined | | unconfined |
|-----------|---|-------------|--|
| | air | propane | propane |
| Comp B | 0.37 (8-c) 0.37 (9-c) | 0.37 (25-c) | 0.33 (37-c) 0.27 (41-c) 0.30 (42-c) 0.36 (43-c) 0.34 (44-c) (Avg. 0.33) |
| Pentolite | 1.04 (10-c) 1.04 (11-c) 1.13 (12-c) 1.13 (13-c) 0.98 (21-c) | | |

Table IV indicates the following:

- (a) Explosive resistivities are of the order of magnitude of one ohm cm.
- (b) There is good repeatability in resistivity values for both explosive materials.
- (c) The effects of confinement and atmosphere for Comp B are not apparent.

A direct comparison of double probe and T probe results is not entirely meaningful since the calculation of resistivity from T probe data neglects any variation of conduction zone geometry with the explosive. In addition, the T probe, due to its size, results in a value of resistivity that is an average or integrated value over the sizeable surface area of the probes. These systematic factors are not present in a double probe measurement. On the other hand, a comparison of the ratios of resistivity for Comp B and Pentolite for each probe type is of interest. Since the procedure for obtaining Pentolite resistivity from T probe data depends upon the arbitrary choice of a reaction zone thickness rather than a systematic interpretation of collected data, as was done for Comp B, this procedure will be deferred until the necessary data for Pentolite is obtained.

A comparison of the above results with that of other investigators is shown in Table V, taken in part from a previous progress report⁽²⁾

Table V

Comparison of Measured Explosive Resistivity (ohm cm)

| | <u>Stevens</u> | | <u>BRL</u> | <u>Utah</u> | <u>LASL</u> | <u>Soviet</u> |
|-----------------|---------------------|----------------|------------|-------------|--|---------------|
| | <u>double probe</u> | <u>T probe</u> | | | | |
| <u>Surface</u> | | | | | | |
| Comp B | 0.95 | 0.33 | 0.29 | -- | -- | 0.2 |
| Pentolite | 1.78 | 1.06 | 0.89 | -- | -- | -- |
| <u>Internal</u> | | | | | | |
| Comp B | 0.94 | -- | -- | 2.56 | 0.24 at 0.5 μ s 0.056 at 0.08 μ s | |

An interesting observation can be extracted from the above presentation. Probes can be classified as having a large or small geometry if the ratio of a characteristic probe dimension to the reaction zone thickness is much greater than or approximately equal to unity, respectively. The characteristic probe dimension employed is a linear dimension of the probe electrode that contributes to the conduction during the measurement. Under this classification the double probe geometry used by the Stevens and Utah groups is a probe of small geometry, while the other probes are considered to be of large geometry. A regrouping of the data in Table V in accordance

(2) Quarterly Progress Report, October - December 1960

with probe classification is shown below in Table VI. The values indicated are simply averages of combined results from all investigators, internal and surface measurements are not distinguished. The resistivity value of the Utah group is omitted due to the stated large uncertainty in probe calibration.

Table VI
Dependence of Measured Resistivity on Probe Geometry
(Resistivity in ohm cm)

| Explosive | Probe Geometry | |
|-----------|----------------|-------|
| | large | small |
| Comp B | 0.27 | 0.95 |
| Pentolite | 0.96 | 1.79 |

It appears that the resistivity values derived from small geometry probe measurements are systematically larger than values derived from large geometry probe measurements. The reason for this systematic variation is not clear. It may be due to probe-explosive shock interactions, or the tendency of large probe geometry measurements to integrate or average the resistivity results.

D. Shaped Charges

The objective of firings 97 and 98 was to observe the collision of two copper jets at a reduced pressure in a propane atmosphere, and ascertain that the collision region is luminous, as was observed with prior firings in air. The observation of a luminous region in and about the point of collision in a propane atmosphere suggests that an energy conversion mechanism rather than a gas shock is responsible for the generated luminosity. The experimental setup, in both firings, consisted of a lucite tube into which copper cones were inserted and the explosive material cast, as shown in Fig. 2. This arrangement provides for a self-contained vacuum chamber and alignment of the opposing copper cones. The system could be flushed repeatedly with propane by alternately pumping and refilling with propane.

Firing 97 yielded no results since one of the detonators failed and no jet collision occurred.

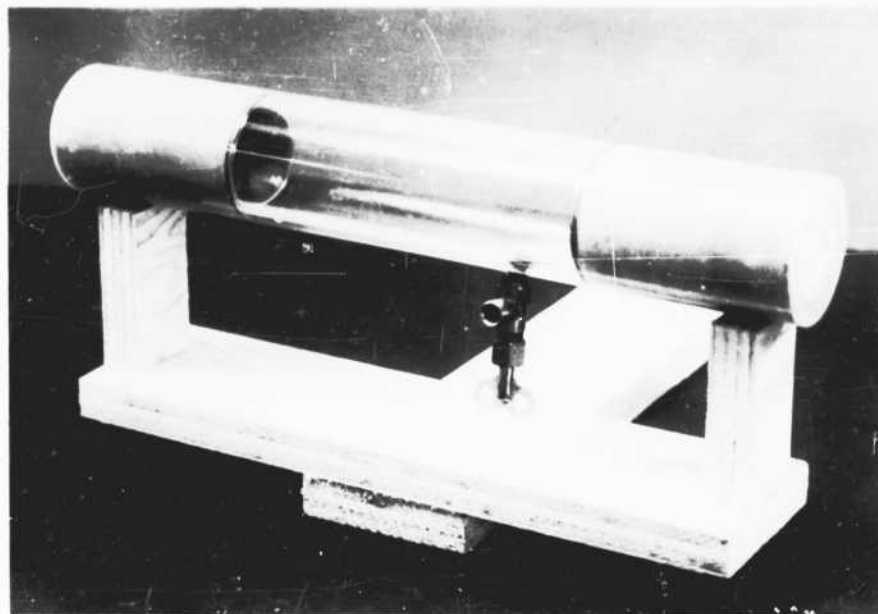


Figure 2

Lucite tube explosive assembly

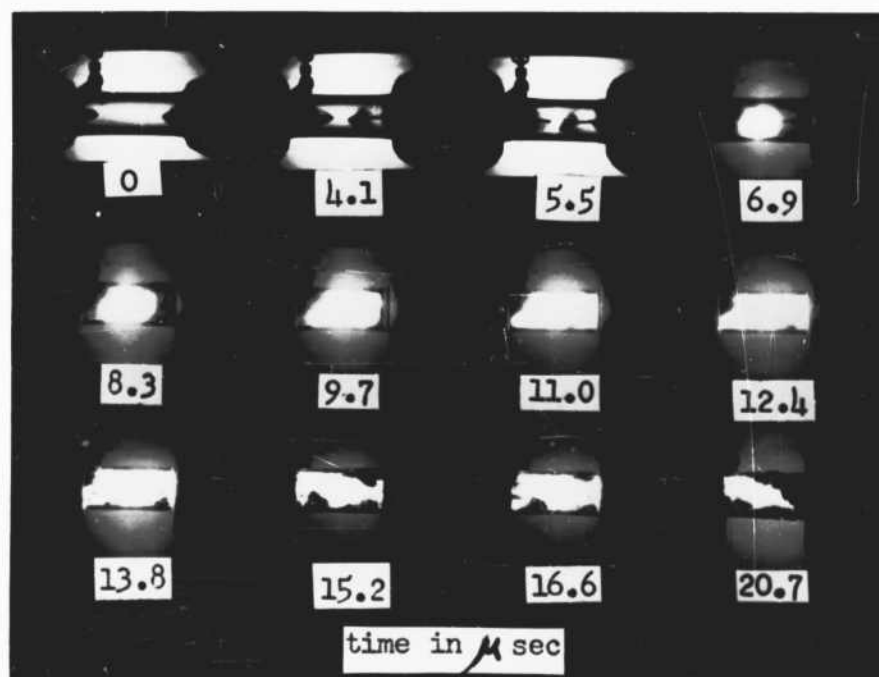


Figure 3

Portions of framing camera record of jet collision
in a low pressure propane atmosphere (arbitrary
zero time reference)

In firing 98 a jet collision was observed. The final pressure in the system was 0.3 mm Hg after five flushing operations. Selected portions of the framing camera record for this firing are shown in Fig. 3 (the zero time reference is arbitrary). No light is observed until the jets first collide, after which the luminous region rapidly fills the volume of the lucite tube. The tube remains luminous for about $7\mu\text{s}$. The latter frames of the record indicate a rapid darkening at various positions along the tube and finally, a bulging and eventual rupture of the lucite chamber.

A prism spectroscope was used to record the spectral content of the luminosity. The intent of firing 99 was to check out the spectrograph and associated instrumentation by observing a jet collision in air, preparatory to firing a lucite-tube explosive assembly. Two opposing shaped charges were set up together with baffles to prevent light from the detonating explosive and background sunlight from entering the spectrograph. The streak camera record indicated a jet collision, midway between the explosive charges. Figure 4 is a reproduction of the spectral record for the collision in air, together with a densitometer scan showing variations of light intensity with wavelength.

The densitometer trace shows two major features; a spectral intensity distribution roughly Planckian in shape, and superposed weak absorption lines. The blackbody curve that best fits the observed spectral distribution, over a wavelength range from 3700 \AA to 4900 \AA , corresponds to a maximum wavelength of about 4225 \AA , and, hence, a color temperature of 6850°K . Since the collision occurred in air, the relative contribution to the spectral data due to air-shock luminosity is not known. If this contribution is large then the above temperature estimate refers to conditions in the air-shock region rather than for the collision.

Table VII is a list of observed absorption line wavelengths that can be identified with lines in the spectrum of copper. The state of ionization of the copper atom associated with the spectral line is also indicated; the notation I and II, is used to designate the source of the line as being from the neutral atom or the singly ionized state, respectively. The accuracy of wavelength determination varies from five to ten angstroms over the observed spectral range.

In firing 100 a jet collision in a vacuum was observed using a lucite-tube explosive assembly. The pressure in the system prior to

Table VII
Absorption Lines in Spectrum of Collision In Air
(Wavelengths in Angstroms)

| Observed Wavelength | Copper* Wavelength | Source | |
|---------------------|--------------------|--------|----------------------------|
| 4017 to 4027 | 4023 | I | very broad abs. line |
| 4067 | 4063 | I | sharp abs. line |
| 4272 to 4280 | 4275 | I | weak, broad abs. line |
| 4513 | 4507 | I | weak, very broad abs. line |
| | 4509 | I | |
| 4573 to 4587 | 4587 | I | broad abs. line |
| 4646 | 4651 | I | sharp abs. line |
| 4682 | 4675 | II | very weak, broad abs. line |
| | 4682 | II | |
| 4698 to 4709 | 4697 | I | sharp abs. line |
| | 4704 | I | |

* Handbook of Chemistry and Physics, 38 ed. (1956-1957)

firing was 80 μ Hg, after five flushing cycles with propane. The framing camera record shows evidence of the collision and is similar in appearance to that shown in Fig. 3. A reproduction of the spectral record and densitometer scan for this experiment is shown in Fig. 5.

In contrast to the spectral results obtained for a jet collision in air, the spectral intensity distribution for the vacuum collision could not be readily matched to a blackbody curve. The intensity distribution is more uniform for the vacuum collision. This suggests that the apparent blackbody distribution for the collision in air is strongly influenced by air-shock luminosity and light from hot detonation gas products. Thus the estimated blackbody temperature is probably not descriptive of conditions in the immediate area of the collision. The extended response at longer wavelengths for the vacuum collision is the result of using a different type of spectrographic plate than that used for the collision in air. The increase in intensity at the red end of the spectrum is believed to be due to incomplete masking of the light from the detonating explosive and hot reaction products.

The number of superposed absorption lines has greatly increased, and many show strong absorption profiles. Table VIII is a list of observed absorption line wavelengths grouped into three categories. The first category (a) contains lines that have strong, sharp profiles and are

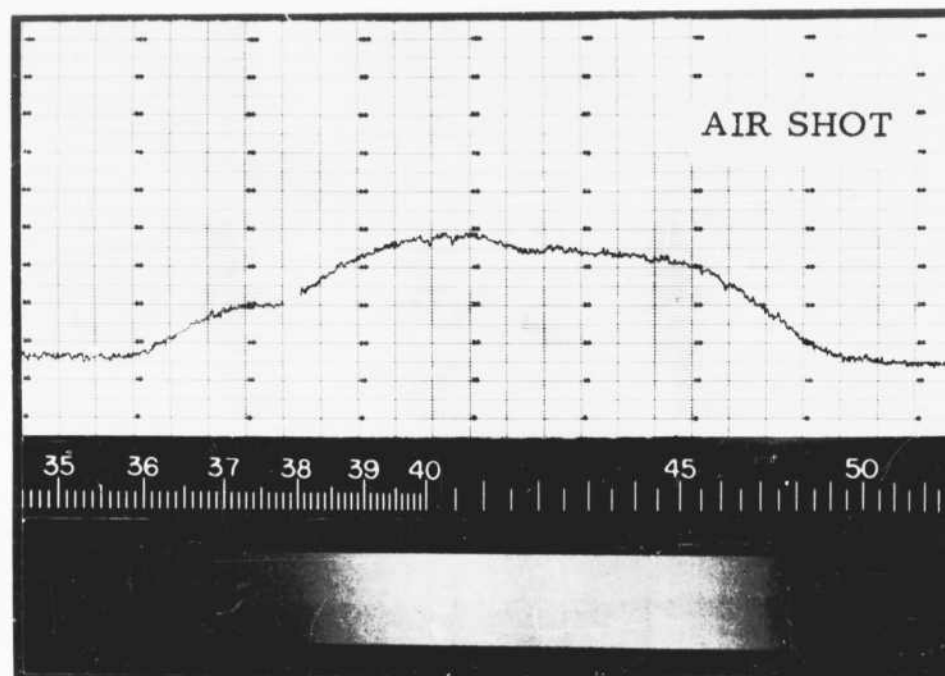


Figure 4

Spectrum and densitometer trace
for jet collision in air

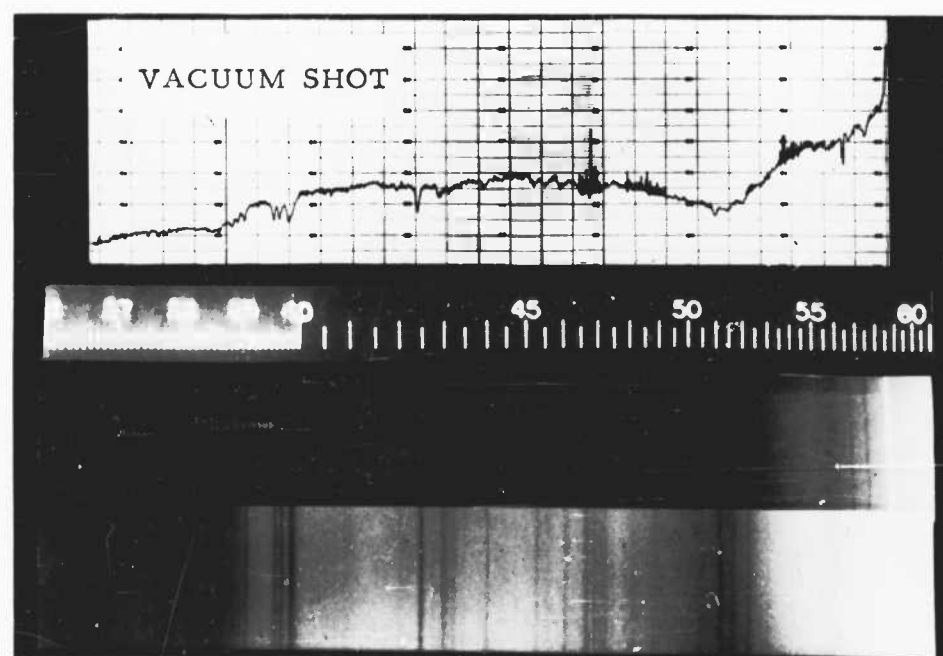


Figure 5

Spectrum and densitometer trace for jet
collision in low pressure propane atmosphere

Table VIII
Absorption Lines In Spectrum of Collision In Vacuum
(Wavelengths In Angstroms)

| (a) | | | (b) | | | (c) | |
|------------------------|----------------------|--------|------------------------|----------------------|--------|------------------------|--------|
| Observed Wavelength | Copper Wavelength | Source | Observed Wavelength | Copper Wavelength | Source | Observed Wavelength | Origin |
| 3710 | 3712 | I | 3800 | 3801 | I | 3718 | - |
| 3740 | 3741 | I | 3864 | 3860 | I | 3724 | - |
| | 3743 | I | | 3862 | I | 3728 | - |
| 4063 | 4063 | I | 4003 | 4003 | I | 3853 | - |
| 4175 | 4178 | I | 4042 | 4044 | II | 3874 | - |
| 4275 | 4275 | I | 4048 | 4051 | I | 3927 | - |
| 4378 | 4378 | I | 4073 | 4073 | I | 3939 | - |
| 4507 | 4506 | II | 4122 | 4122 | I | 3959 | - |
| | 4508 | I | | 4123 | I | 3991 | - |
| | 4509 | I | 4478 | 4480 | I | 4092 | - |
| 4531 | 4531 | I | 4682 | 4682 | II | 4222 | - |
| 4538 | 4540 | I | 4928 | 4932 | II | 4295 | - |
| 4583 | 4587 | I | 5052 | 5052 | II | 4628 | - |
| 4674 | 4675 | II | 5057 | 5059 | II | 4783 | - |
| 4708 | 4705 | I | | 5061 | II | 4852 | - |
| 5104 | 5106 | I | 5068 | 5065 | II | 4891 | - |
| 5153 | 5153 | I | | 5067 | II | 5894 | sodium |
| 5218 | 5218 | I | | 5072 | II | | |
| | 5220 | I | 5089 | 5084 | II | | |
| 5292 | 5293 | I | | 5088 | II | | |
| 5698 | 5700 | I | 5098 | 5094 | II | | |
| 5781 | 5782 | I | 5207 | 5207 | II | | |

Identified with lines in the copper spectrum. The second category (b) contains lines that are weak and show a poorly defined minimum but can also be associated with known copper lines. The stage of ionization of the copper atom associated with the spectral line is also included in parts (a) and (b). The last grouping (c) contains lines with strong, sharp profiles that do not correspond to known copper lines. The accuracy of the wavelength determination varies from about one to five angstroms over the observed spectral range.

In order to identify the sources of absorption lines not associated with lines in the copper spectrum (part (c) of Table VIII), a sample shaped charge copper cone was submitted for a spectroscopic impurity analysis. The total impurity concentration detected was about two hundred parts per million or 0.02%. Since the impurities contained in the copper cone are present only in trace amounts, it is improbable that the strong unidentified absorption lines in the collision spectrum can be attributed to these impurity materials. It seems most plausible to associate these absorption lines with other explosive and inert materials used in the experimental setup, or with chemical derivatives from these materials.

The objectives of firing 101 were as follows: to observe the gross features of the collision of a single copper jet with a massive, stationary copper target in vacuum; to correlate these spectral observations with similar work of Clark, et. al.⁽¹⁾; and to observe the effect of a reduction in the relative impact energy upon the spectral characteristics of the collision. The experimental setup was constructed by inserting a shaped charge assembly into one end of a lucite tube, and sealing the other end with a cylindrical block of copper. The distance between the explosive charge and copper target was approximately half the distance between the explosive charges employed in firing 100.

Figure 6 is a reproduction of portions of the framing camera record for this firing. No light is observed until the jet impacts upon the target, after which the luminous region appears to spread rapidly throughout the remaining portion of the lucite tube. Due to a faulty spectrographic film plate, the spectral characteristics of this collision were not clear and no densitometer intensity profile was obtained. This firing will be repeated at a future date.

(1) J.S. Clark, R.R. Kadesch, R.W. Grow "Spectral Analysis of the Impact of Ultra Velocity Copper Spheres into Copper Targets" Tech. Report No. OSR-13, Univ. of Utah, Sept. 1, 1959.

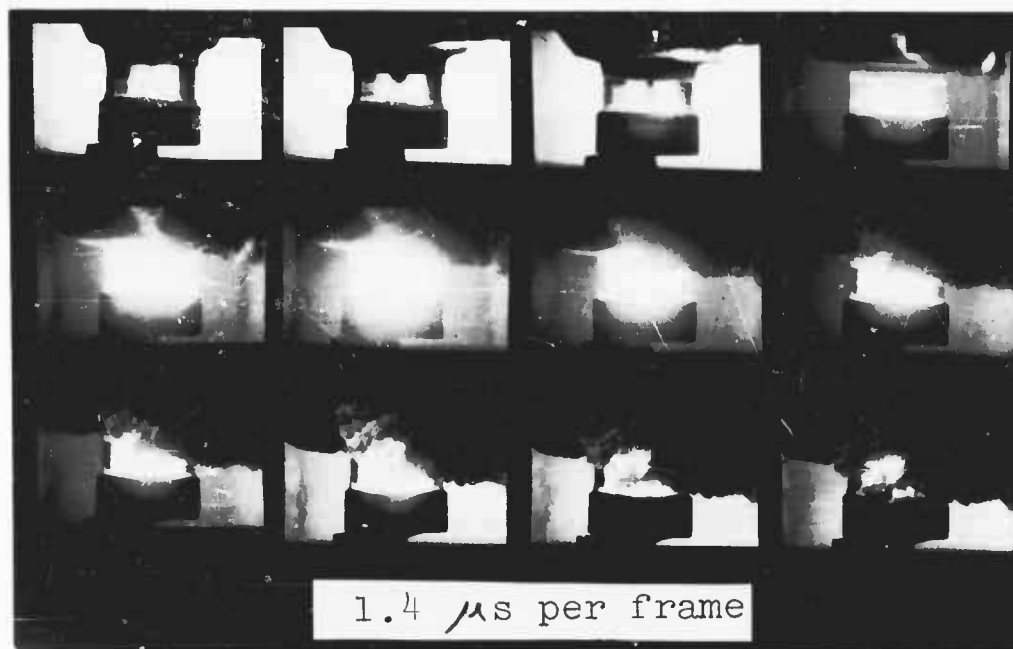


Figure 6

Portions of framing camera record of a
single jet impacting upon a copper target

WORK PLANNED FOR NEXT QUARTER

During the next quarter the final assembly of the capacitor bank will be undertaken. This will include the design of the control and synchronization circuitry for use at the Arsenal firing site. Also, calculations and test firings will be made on portions of the bank structure to assure the adequacy of the mechanical structure under explosive impact loading.

The shaped-charge collision work will be continued with the effort directed toward obtaining a time resolved spectrum. This is necessary to show at what stage of the jet collision the ionized copper appears and whether any ionized copper emission lines can be observed. This will aid considerably in the analysis of the phenomena that are taking place since contamination of the spectrum by air shock luminosity and detonation products can be avoided.

The conductivity firings with 10% seeded charges will continue in order to assess the effectiveness of this approach to achieving magneto-hydrodynamic effects with chemical explosives.

PERSONNEL

Personnel of Stevens Institute of Technology who have been associated with the work reported here are:

Dr. W.H. Bostick

Dr. S. Koslov

Dr. S.J. Lukasik

Mr. B.J. Pernick

Mr. L.H. Weeks

Personnel of Picatinny Arsenal who have contributed to the work are:

Dr. J.V.R. Kaufmann

Mr. A. MacKenzie

Mr. F. Schwartz

Mr. E. Walbrecht

Mr. E. Dalrymple

DISTRIBUTION LIST

Commanding Officer
Diamond Ordnance Fuse Laboratories
Washington 25, D. C.

Technical Reference Section (1)

Commanding General
Aberdeen Proving Ground
Aberdeen, Maryland

BRL - Dr. R. Eichelberger (1)

Chief of Ordnance
Department of the Army
Washington 25, D. C.

ORDTB (1)

Armed Services Technical Information
Agency
Arlington Hall Station
Arlington 12, Virginia (10)

Commanding Officer
Picatinny Arsenal
Dover, New Jersey

Purchasing Office, ORDBB-PBI (5)

Commanding Officer
Office of Ordnance Research
Box CM, Duke Station
Durham, North Carolina

Dr. Sherwood Githen (1)

Explosives Research Laboratory
Bureau of Mines
4800 Forbes Avenue
Pittsburgh 13, Pennsylvania

Dr. F. Gibson (1)

Mr. Laddie L. Stahl
Manager - Technical Relations
General Electric Company
Schenectady, New York (1)

Dr. Arthur H. Guenther
Director, Pulse Power Laboratory
Air Force Special Weapons Center
Kirtland Air Force Base
New Mexico (1)

Dr. David Bernstein
Pouiter Laboratories
Stanford Research Institute
Menlo Park, California (1)